

Roll-to-Roll Dry Transfer of Large-Scale Graphene

Nan Hong, Dmitry Kireev, Qishen Zhao, Dongmei Chen, Deji Akinwande, and Wei Li*

A major challenge for graphene applications is the lack of mass production technology for large-scale and high-quality graphene growth and transfer. Here, a roll-to-roll (R2R) dry transfer process for large-scale graphene grown by chemical vapor deposition is reported. The process is fast, controllable, and environmentally benign. It avoids chemical contamination and allows the reuse of graphene growth substrates. By controlling tension and speed of the R2R dry transfer process, the electrical sheet resistance is achieved as $9.5 \text{ k}\Omega \text{ sq}^{-1}$, the lowest ever reported among R2R dry transferred graphene samples. The R2R dry transferred samples are used to fabricate graphene-based field-effect transistors (GFETs) on polymer. It is demonstrated that these flexible GFETs feature a near-zero doping level and a gate leakage current one to two orders of magnitude lower than those fabricated using wet-chemical etched graphene samples. The scalability and uniformity of the R2R dry transferred graphene is further demonstrated by successfully transferring a $3 \times 3 \text{ in}^2$ sample and measuring its field-effect mobility with 36 millimeter-scaled GFETs evenly spaced on the sample. The field-effect mobility of the R2R dry transferred graphene is determined to be $205 \pm 36 \text{ cm}^2 \text{ V}^{-1}$.

a target substrate for device fabrication. The R2R technique is especially desirable for large-scale graphene transfer, because it is compatible with the high-throughput production of flexible electronics.^[18–21] Previously, the R2R graphene transfer has been achieved via wet transfer processes, including wet chemical etching, hydrogen bubbling, and hot water delamination.^[22–26] Wet chemical etching does not allow recycling of the metal substrate. The hydrogen bubbling and hot water delamination methods require extra equipment for liquid handling, and the process is hard to control. More importantly, these wet transfer methods leave hard-to-remove residues that result in highly doped graphene behavior, which is undesirable for device fabrication.

A R2R dry transfer process was recently developed by Hao et al.^[27] using mechanical peeling to delaminate CVD graphene from its growth substrate. In the process, a polymer-backing layer with adhesive

is first laminated onto as-grown graphene, and the laminate is then peeled with two guiding rollers on a R2R machine. Mechanical peeling of graphene either manually^[28,29] or with a double-cantilever setup^[30,31] has been studied with small graphene samples. The effort to achieve R2R peeling of large-scale CVD graphene has just began.^[27,32–34] The work done by Hao et al.^[27] has demonstrated the feasibility of the R2R method. However, the peeling tensions were not actively controlled, and the quality of the transferred graphene needs to be dramatically improved to be comparable to that of wet-chemical etched samples.^[35]

In this work, we develop a new system for R2R dry transfer of large-scale graphene with simultaneous control of peeling tension and speed. A systematic experimental study is conducted to examine process parameter effects and to identify the optimal process condition. The R2R dry transfer process can achieve an equivalent sheet resistance of $9.5 \text{ k}\Omega \text{ sq}^{-1}$, the lowest value ever reported for R2R dry transferred graphene samples. We also use the dry transferred graphene to fabricate flexible graphene-based field-effect transistors (GFETs). It is demonstrated that these GFETs have a relative leakage current I_{GS}/I_{DS} almost 100 times lower than those fabricated with wet-chemical etched graphene, suggesting the uncontaminated nature of the R2R dry transferred graphene samples. Furthermore, the developed R2R system is used to dry-transfer a 3-in. \times 3-in. graphene sample, and the transfer uniformity is demonstrated with the field-effect mobility characterization.

1. Introduction

Graphene, a carbon allotrope with a 2D honeycomb lattice, has received widespread attention due to its unique band structure and extraordinary material properties,^[1–4] including high electron mobility, optical transmittance, thermal conductivity, mechanical strength, and biocompatibility.^[4–9] These remarkable properties lend graphene a compelling material for many potential applications, such as organic solar cells, biocompatible sensors, filtration membranes, light-emitting diodes, and flexible touchscreens.^[10–13] Large-scale graphene growth has been demonstrated with roll-to-roll (R2R) chemical vapor deposition (CVD), where monolayer graphene is grown on transition metals such as copper and nickel.^[14–17] After the growth, graphene needs to be transferred from the growth substrate to

N. Hong, Q. Zhao, D. Chen, W. Li
Walker Department of Mechanical Engineering
University of Texas at Austin
Austin, TX 78712, USA
E-mail: weiwli@austin.utexas.edu

D. Kireev, D. Akinwande
Department of Electrical and Computer Engineering
University of Texas at Austin
Austin, TX 78712, USA

 The ORCID identification number(s) for the author(s) of this article can be found under <https://doi.org/10.1002/adma.202106615>.

DOI: 10.1002/adma.202106615

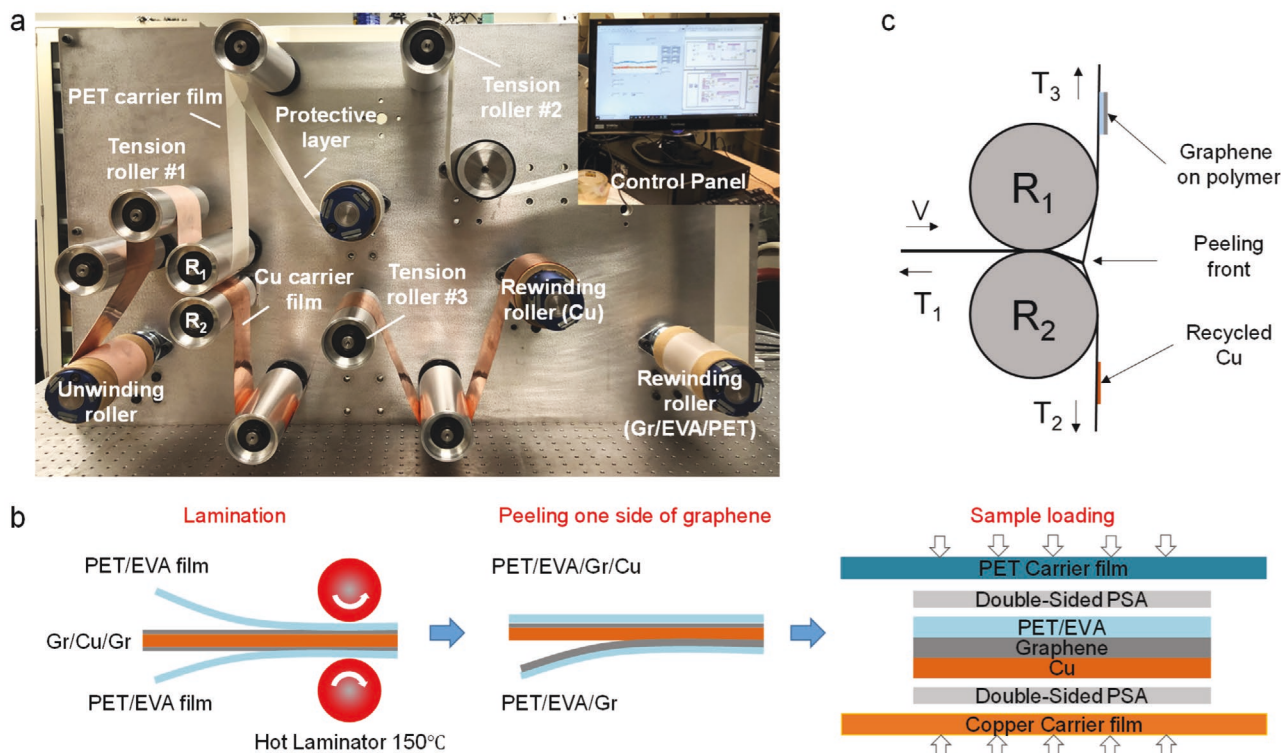


Figure 1. The R2R graphene dry transfer process and sample preparation procedure. a) Front view of the R2R graphene transfer system with the control panel. b) Sample lamination and loading. c) Mechanical peeling front, where V is the linear film speed, and T_1 , T_2 , and T_3 are the tension forces on the webs before and after peeling.

2. The Roll-to-Roll Dry Transfer Process

The R2R dry transfer process is illustrated in **Figure 1**. The mechanical peeling action was controlled with three motors: one on the unwinding roller to control the web speed and two on the rewinding rollers to control the web tensions (Figure 1a). Three idler rollers were instrumented with loadcells to monitor the tensions in the webs. The graphene samples used in this work were $100 \times 100 \text{ mm}^2$ CVD-grown monolayer graphene on copper foil, first laminated with polyethylene terephthalate/ethylene vinyl acetate (PET/EVA) film and then cut into $30 \times 10 \text{ mm}^2$ specimens (Figure 1b). Smaller specimens were used in the transfer experiments to reduce the material cost. The specimens were again laminated in between carrier films and the polymer-graphene-copper laminate was peeled with two guiding rollers R_1 and R_2 (Figure 1c). By controlling the tension forces (T_2 , and T_3) and the linear web speed (V), peeling is maintained at the graphene and copper interface, transferring graphene from the copper substrate to the polymer film. The copper foil is then collected by a rewinding roller, and the graphene-on-polymer sample is collected by the other.

3. Characterization of Transferred Graphene

We evaluated the quality of the transferred graphene samples by measuring their electrical sheet resistance. To ensure that the transferred graphene is pristine, an array of thin metal pads (90 nm Au and 10 nm Ni) were evaporated through a shadow

mask and used as electrodes for resistance measurements, as shown in **Figure 2**. The electrodes were $1.25 \times 1.25 \text{ mm}^2$ and 1.25 mm apart. A four-probe measurement technique was used to eliminate the contact resistance between graphene and the conductive pads. With the array of electrodes, resistances at different locations and on both directions (R_x and R_y) of the sample could be measured, such that the uniformity of dry transferred graphene could be analyzed with the peeling conditions.

However, even if the quality of transferred graphene were uniform, the resistance measurements at different locations within the sample would not be the same due to the edge effect of the electric field distribution during the resistance measurements (Figure S1, Supporting Information). A correction factor was needed before the electric resistance measurements could be used to compare the process parameter effect. In this study, wet-chemical etched graphene samples were used to obtain correction factors at different locations of the dry peeled samples. The same metal pad array was made on wet-chemical etched samples of the exact same dimensions as the dry peeled samples. The resistance measurement in the X direction at the center of the sample was used as a basis, and the measurements at all other locations were normalized against this base value to yield the correction factors for different locations on the sample, as shown in Figure 2b. Since the quality of wet etched samples can be assumed uniform, the difference among the surface resistance measurements is only caused by the edge effect. Therefore, the corrected surface resistance measurements at different locations of the dry transferred samples reveal the uniformity of the transfer quality as a result of

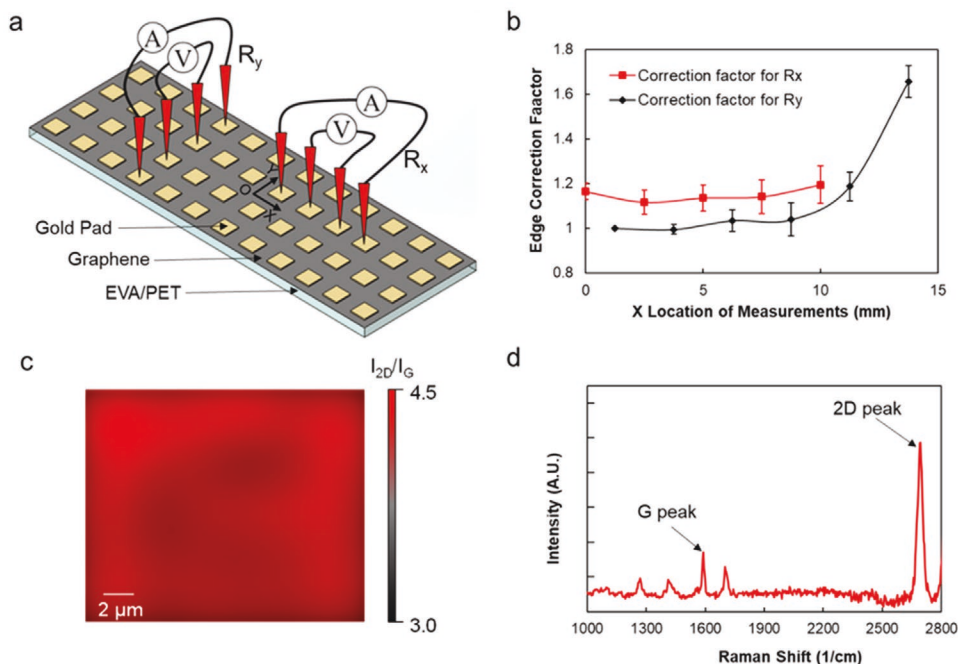


Figure 2. Resistance measurement method and edge effect. a) A schematic of the four-probe resistance measurement method used in this study. b) Correction factors for R_x and R_y at different locations. c) Raman map of I_{2D}/I_G ratio. d) Raman peaks of dry transferred graphene on PET/EVA.

the process parameters. As seen in Figure 2b, the correction factor could be as large as 1.7 for R_y and 1.2 for R_x at their corresponding edge locations. To confirm these edge effect correction factors, a finite element simulation model was developed in COMSOL. The simulation results matched closely with the experimental results (Figure S1, Supporting Information). Figure 2c shows a Raman map of dry transferred graphene. The I_{2D}/I_G ratio is all above 3, indicating high-quality monolayer graphene is obtained. Figure 2d is a typical Raman scan of dry transferred graphene on the PET/EVA substrate.

4. The Effects of Peeling Tension and Peeling Speed

The edge-effect corrected sheet resistance measurements of transferred graphene are used to analyze the effects of peeling tension and peeling speed. Comparing resistances along the X and Y directions, i.e., R_x and R_y , no significant difference has been found (Figure S2, Supporting Information); therefore, only R_y is used in the analysis. The effect of both the peeling speed and the peeling tension can be seen in Figure 3. Both the speed and tension significantly affect the transferred graphene quality. When the peeling speed is low, there is significant variation among the surface resistance measurements along the peeling direction of the graphene sample. This trend is observed regardless the peeling tension levels. As the speed increases, the quality of the transferred graphene tends to be more uniform, except for the high peeling force case at 15 N (Figure 3c). At a higher peeling force, more cracks could form at the grain boundaries of transferred graphene, causing more randomness and higher resistance in the transferred graphene samples. Similar findings have also been reported in a previous study.^[36]

Taking the sample average of all resistance measurements under each tension and speed condition, we examined the overall effects of tension and speed (Figure 3d). At the lower tension levels of 5 and 10 N, the average sample resistance reaches a minimum value when the speed is at about 2 m min⁻¹. However, at the high force level of 15 N, there is a decreasing trend as the speed increases. Previous studies^[30,37] have found that the adhesion energy at bonding interfaces is rate-dependent. The difference between the adhesion energy at the graphene and PET/EVA interface and that at the graphene and copper interface varies with the peeling speed. A large adhesion energy difference between the two interfaces leads to easier separation of graphene from the copper substrate. However, a higher adhesion energy requires a higher peeling force, which in turn could cause damage to graphene and thus higher surface resistance measurements. Therefore, there could be an optimal peeling speed to achieve the lowest surface resistance, as seen in the 5 and 10 N cases. However, when the peeling force is at 15 N, the peeling speed is not high enough to reach the optimal peeling condition.

To determine the quality of transferred graphene, both the average and standard deviation of the sheet resistance need to be considered. A low average resistance value is required for electronic applications, while a low standard deviation represents the consistency of the R2R dry transfer process. Figure 4 shows a Pareto Frontier chart of the peeling conditions. The chart can be divided into four regions. In Region I, the low peeling speed of 0.5 m s⁻¹ resulted in high average resistances and high process variations regardless of the peeling forces. In Region II, the transferred graphene quality is slightly improved with higher peeling speeds. The transferred graphene quality in Region III was further improved, with a combination of

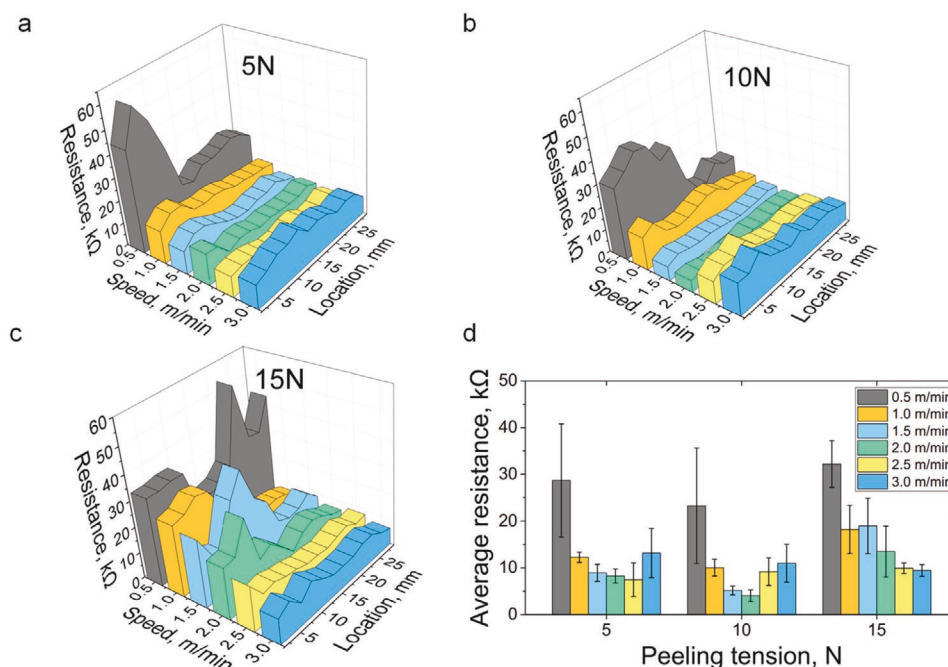


Figure 3. Surface resistance variation of transferred graphene samples when peeling force is at a) 5 N, b) 10 N, and c) 15 N. d) Average resistance of transferred graphene under different peeling conditions.

moderate tension and speed conditions. The most desirable conditions were obtained in Region IV, where the 2 m min^{-1} and 10 N condition yielded the lowest average resistance. However, the 1.5 m min^{-1} and 10 N condition yielded the second-lowest average resistance and the lowest standard deviation. Regression models were developed to identify the optimal peeling condition using the average resistance as a response variable (Table S1, Supporting Information). A third-order regression model was used to conduct process optimization. The optimal peeling condition was found to be 1.8 m min^{-1} and 12 N (Figure S3, Supporting Information), which matches the result from the Pareto Frontier analysis. Figure 4b shows the SEM images of transferred graphene obtained using these two conditions. Both samples have larger than 99% graphene coverage.

The sheet resistance of dry transferred graphene samples obtained at 2 m min^{-1} and 10 N was compared with that of wet-chemical etched samples. The same electrode patterns were made on a wet etched sample. A ratio of R_{y-d}/R_{y-w} was calculated at corresponding locations of the two samples, where R_{y-d} and R_{y-w} were the resistance measurements from the dry peeled and wet etched sample, respectively. Excluding the first and last two measurements, which could be unreliable because of sudden changes of the peeling process at the start and end of the sample, the average R_{y-d}/R_{y-w} ratio is found to be 2.7 (Figure S4, Supporting Information). This means that the surface resistance of R2R dry transferred graphene is only 2.7 times that of the wet etched one. To compare with other reports, the sheet resistance of wet etched monolayer graphene on PET/EVA was measured with a $1 \times 1 \text{ cm}^2$ sample using the standard van der Pauw four-probe method. The sheet resistance of the wet etched sample was measured as $3.5 \text{ k}\Omega \text{ sq}^{-1}$; therefore, the sheet resistance of the R2R dry transferred graphene

obtained in this study is determined to be $9.5 \text{ k}\Omega \text{ sq}^{-1}$ ($= 2.7 \times 3.5 \text{ k}\Omega \text{ sq}^{-1}$).

5. Graphene-Based Field Effect Transistors with R2R Dry Transferred Graphene

The dry transferred graphene obtained from this study was used to fabricate flexible GFETs, and their performance was compared with that of GFETs fabricated with wet etched graphene samples. Since its discovery, major efforts have been devoted to research and technological development of making functional devices based on graphene. Graphene field-effect transistors are among the most needed and yet most challenging to fabricate via high-quality CVD-grown graphene.^[38] In this study, the graphene samples dry peeled at 10 N and 2.0 m min^{-1} were embossed onto a prestructured gold/EVA/PET substrate. The resulting stack contains high-quality graphene with gold contacts that are self-passivated with EVA/PET, as shown in Figure 5. The gold interdigitated electrodes (IDE) were fabricated with a mechanical cutter plotter (Silhouette Cameo). The IDE and graphene were covered with another PET layer that is ultrathin, insulating them from the environment. This construction is ideal for electrolytic gating, essential for high-quality, low-noise chemical, and biosensing.^[39]

Figure 5a shows the fabrication schematic of the GFETs. Figure 5b shows typical $I_{DS}-V_{GS}$ curves of three GFETs fabricated with R2R dry transferred graphene. There are three essential features of the R2R GFETs. The first is the near-zero doping of the dry transferred graphene, which is observable by the location of the Dirac point (V_{dirac}) of the GFET. In most of the wet-etch-based GFETs, the V_{dirac} point is located at $350 \pm 100 \text{ mV}$ due to the p -doping induced by the copper etchant. To

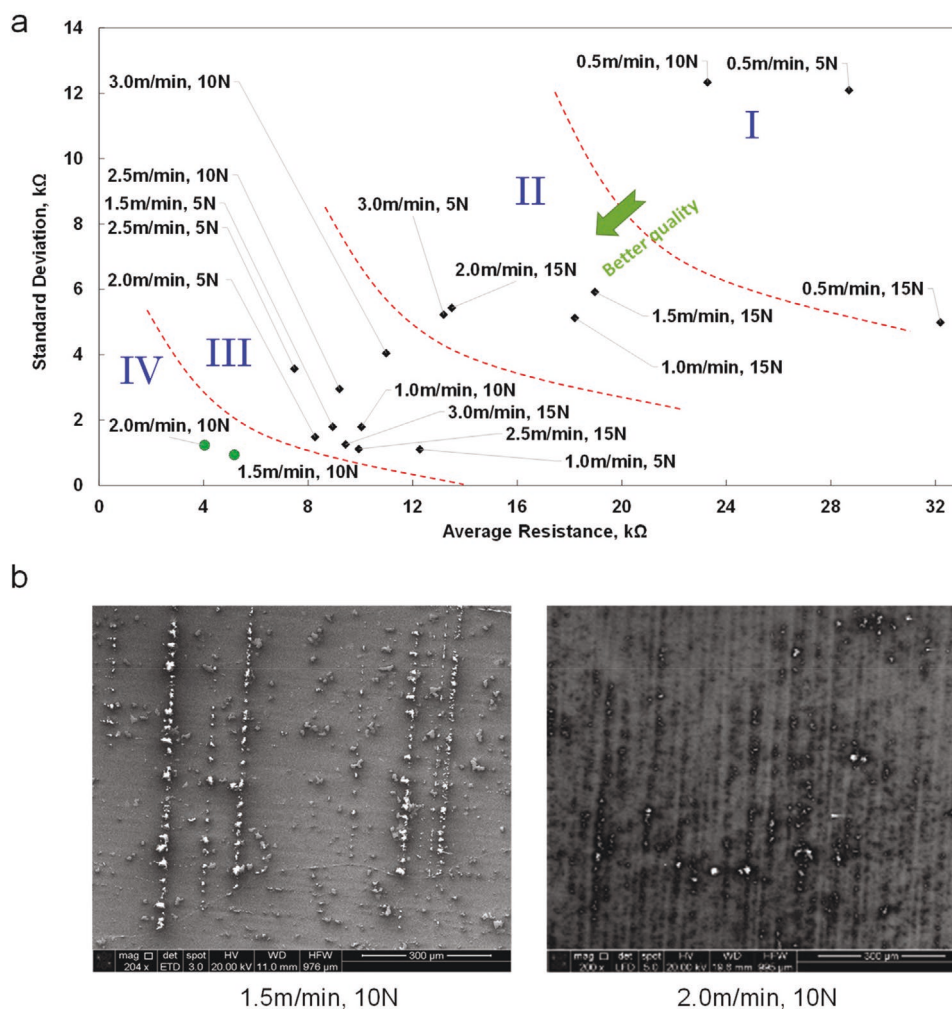


Figure 4. a) A Pareto Frontier plot of the R2R graphene dry transfer process. b) SEM images of transferred graphene on PET/EVA under the two identified peeling conditions.

directly compare our R2R GFETs with those fabricated using wet etched graphene samples, we transferred the same graphene via wet etching in ammonium persulfate onto polyimide (PI, Kapton) and PET with PMMA as a temporary polymer support. Identical IDE structures of gold/EVA/PET were bound on top of these graphene/Kapton and graphene/PET target substrates. The $I_{DS}-V_{GS}$ curves for wet-etched samples are shown in Figure S5, Supporting Information. Drastic differences in the doping level have been observed in these two types of devices (Figure 5c). The V_{dirac} points are approximately 300 and 400 mV for the wet transferred graphene/PET (wet PET) samples and the wet transferred graphene/Kapton (wet PI) samples, respectively, while it is almost 0 mV for the R2R dry transferred (dry R2R) samples. The transconductance of the dry R2R GFETs is unfortunately lower compared with the wet PET and wet PI GFETs (Figure 5d). This could be due to the presence of defects in the dry transferred graphene. Nonetheless, transconductance is not the only important parameter of a GFET. One peculiar and common issue with the GFETs is the large gate leakage current. The issue is less prominent when it comes to micro/nanoscale processed high-quality GFETs because of

specific and thorough feedline passivation. However, the passivation step can be challenging when fabricating low-cost and flexible GFETs in mass production. Gate leakage current can cause reduced device performance and sensing specificity. In this work, we achieved excellent self-passivation with the sandwich structure of dry transferred PET/EVA/graphene and gold/EVA/PET. As shown in Figure 5e, the relative leakage current I_{GS}/I_{DS} at the Dirac potential for the R2R GFETs is almost 100 times lower than the wet PET GFETs and more than an order of magnitude lower compared with the wet PI GFETs. This clearly indicates that the dry peeled R2R GFETs are effectively passivated, and the gate leakage current is minimal in these devices.

It is also important to note here that the relatively low transconductance of the dry-transferred samples shown in Figure 5d and, for that matter, their relatively high resistance of $9.5 \text{ k}\Omega \text{ sq}^{-1}$ as compared with those of wet-transferred samples is because of different doping levels in these samples. The resistance measurements of near-zero-doped graphene samples using the two-probe or four-probe technique often yield values 10–50 times that of highly doped ones, since the readings will correspond to the charge neutrality point, i.e., the highest resistivity

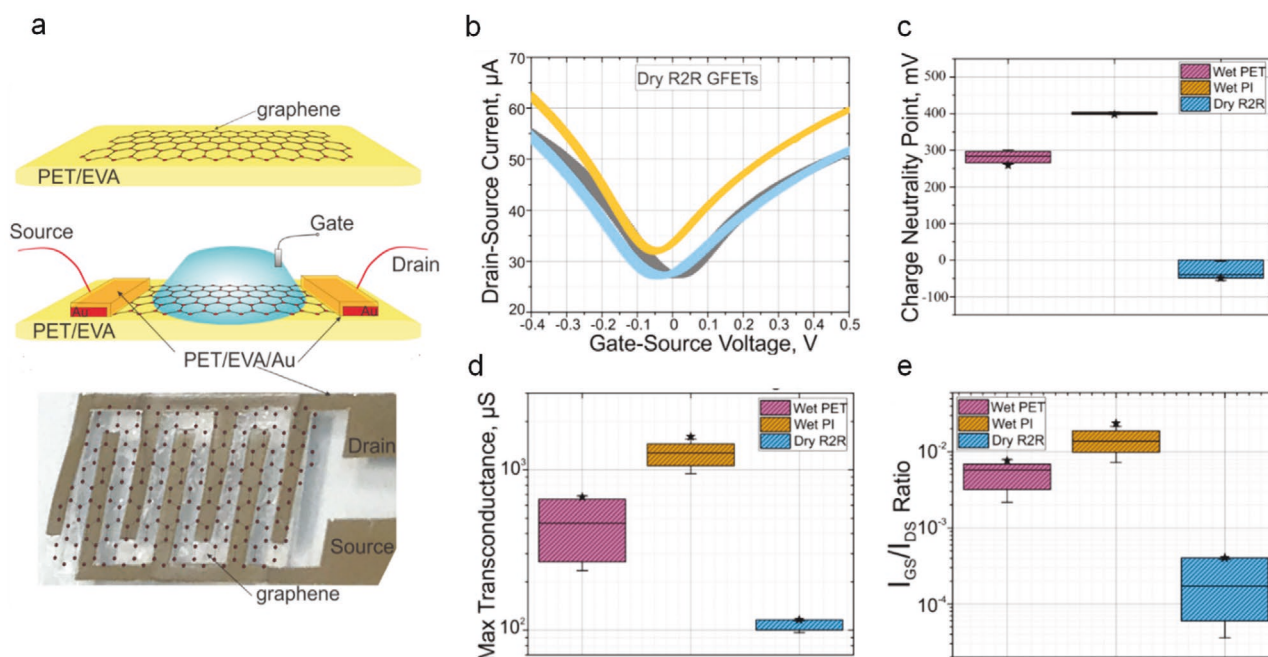


Figure 5. a) Fabrication of the graphene-based field effect transistors. b) $I_{DS}-V_{GS}$ curves of three dry R2R GFETs. c) Comparison of the charge neutrality point (doping level) of dry-R2R and wet-transferred devices. d) Comparison of the max transconductance among three different type of graphene samples. e) Comparison of relative values of gate current leakage.

point of the monolayer graphene in a field-effect mobility test. For wet-etched graphene samples that are normally doped, the resistance measurements without a gate voltage would correspond to a point away from the charge neutrality peak, yielding a much lower resistance reading. The R2R dry-transferred graphene samples have a near-zero doping level. Their electrical resistance can be dramatically reduced by doping.

6. Mobility and Uniformity of R2R Dry Transferred Graphene

To further demonstrate the scalability of the developed R2R dry transfer process, a 3-in. \times 3-in. CVD graphene sample was transferred from copper to PET/EVA using the process condition 10 N and 2.0 m min^{-1} . Figure 6a shows the graphene on copper sample, with the upper two corners slightly deformed due to handling. Figure 6b shows the transferred graphene on PET/EVA sample, which remains transparent. The transferred graphene/EVA/PET sample was cut into an array of 6 \times 6 pieces for GFETs fabrication. Two pieces of gold-on-polymer material were placed on the graphene/EVA/PET sample as source and drain electrodes of the GFET. The two electrodes formed a 3 mm (L) \times 5 mm (W) graphene conductive channel. For convenience, a simple gel electrolyte material (3M Red Dot) was placed on top of the source and drain electrodes as the gate.

The field-effect mobility μ is determined based on the following equation^[38]

$$\mu = \frac{L}{W} \frac{g_m}{C_{\text{int}} V_{\text{DS}}} \quad (1)$$

where L is the channel length and W is the channel width. The transconductance g_m can be calculated with the measured $I_{DS}-V_{GS}$ curves. C_{int} is the interface capacitance between the electrolyte and graphene, which was determined to be 2.0 $\mu\text{F cm}^{-2}$ previously.^[38,40,41] V_{DS} is the voltage applied to the source and drain. Figure 6c shows a mobility map generated with measurements from all the 36 GFETs evenly distributed on the 3-in. \times 3-in. graphene sample. The field effect mobility was found to be in the range of 130–260 $\text{cm}^2 \text{V}^{-1} \text{s}^{-1}$, with a highly uniform distribution in most of the areas. The two regions with relatively low mobility values coincided with those of deformed areas on the graphene-on-copper sample before the transfer, suggesting that the low mobility was caused by mechanical damage during the sample handling process. Figure 6d shows the mobility variation along the peeling direction. It is seen that the transferred graphene quality in the peeling start area was relatively low compared with the rest of the sample. This was due to the sudden start of the peeling process.

The overall field effect mobility of the R2R dry transferred sample is compared with those from other studies to benchmark the effectiveness of the R2R dry transfer process, as shown in Figure 6e. The first column shows the mobility measurement results of the 3-in. \times 3-in. sample from this work. The second column are the measurements of wet transferred samples with PMMA using the same mobility measurement method. The third column is the data from Abhay et al.,^[28] where a dry transfer method of CVD graphene on copper foil was demonstrated with polyvinyl alcohol (PVA) by manual peeling. The last column is the data from Caldwell et al.^[42] for dry transferring epitaxial graphene onto arbitrary substrates. Although the mobility of the R2R dry transferred sample is not as high as some of the previously published values, it is important

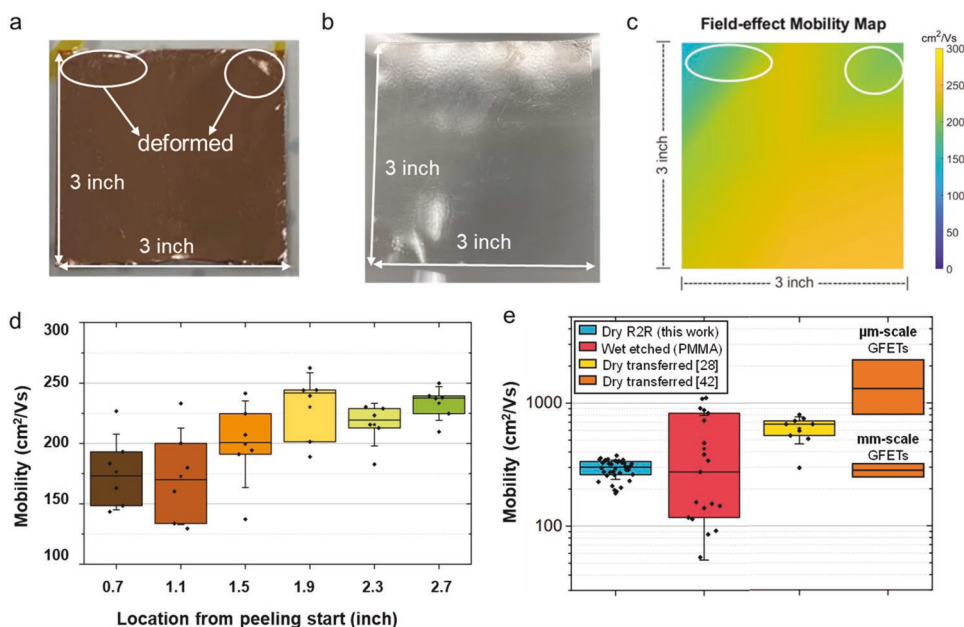


Figure 6. a) Image of a 3-in. × 3-in. monolayer graphene on copper sample. b) Image of the transferred graphene on PET/EVA sample. c) Mapping of the field-effect mobility of the 3-in. × 3-in. transferred graphene/EVA/PET sample. d) Mobility variation as a function of location from the peeling start point. e) Comparison of mobility values among the R2R dry transferred samples, wet etched graphene-on-PMMA samples, and the reported values.^[28,42]

to note that the mobility measurements in this study were obtained with GFETs of a much larger channel size, on the level of $3 \times 5 \text{ mm}^2$. Most of the previous studies fabricated microscale and nanoscale graphene channels for mobility measurements. Such small channel sizes allow high probability to make a GFET on a single grain of graphene. Thus, the mobility measurements would be extremely high. As the channel size of GFETs increases, the obtained mobility value will be substantially smaller, as has been reported in Caldwell et al.^[42] The mm-scale GFETs had a mobility value about one-fourth that of μm -scale GFETs, as can be seen in Figure 6c. With a comparable GFET channel size, the field effect mobility of dry-transferred graphene obtained in this study is on the same level as the previously published data. The average mobility over the entire 3-in. × 3-in. graphene sample is found to be $205 \pm 36 \text{ cm}^2 \text{ V}^{-1} \text{ s}^{-1}$, demonstrating the uniformity of the R2R dry transferred graphene obtained in this study.

7. Conclusion

In summary, a R2R dry transfer process with simultaneous peeling speed and tension control is developed for large-scale CVD graphene transfer. Experiments were conducted to examine the process parameter effects and to identify the optimal process condition. The R2R dry transferred graphene was used to fabricate flexible GFETs that can be used as biochemical sensors. The optimal process condition in the study yielded a surface resistance of $9.5 \text{ k}\Omega \text{ sq}^{-1}$, on the same order comparing to wet etched graphene samples from the same source. The flexible GFETs fabricated with the R2R dry transferred graphene had a near-zero doping level and a gate leakage current about 100 times lower compared with those fabricated

using wet etched graphene samples. Large-scale graphene transfer was also conducted using a 3-in. × 3-in. CVD graphene-on-copper sample. Thirty-six GFET devices were made using the transferred graphene evenly spaced across the whole sample. All the GFETs were electrically conductive, yielding an overall field effect mobility value of $205 \pm 36 \text{ cm}^2 \text{ V}^{-1} \text{ s}^{-1}$. This study demonstrates the potential of the proposed R2R dry transfer process for high-quality and large-scale graphene applications.

8. Experimental Section

The graphene samples used in this work were CVD-grown monolayer graphene on $25 \mu\text{m}$ thick copper foil provided by GrollTex (San Diego, CA). Graphene samples of $100 \times 100 \text{ mm}^2$ were first laminated with polyethylene terephthalate/ethylene vinyl acetate (PET/EVA) film to make a five-layer sandwiched structure, PET/EVA-graphene-Cu-graphene-EVA/PET. The sandwiched sample was then cut into $30 \times 10 \text{ mm}^2$ specimens. Smaller specimens were used in the graphene transfer experiments to reduce the material cost. The PET/EVA/graphene on one side of the copper foil was manually removed, and the other side of the specimen was bonded in between a roll of PET carrier film (MYLAR A, $254 \mu\text{m}$ thick) and a roll of copper carrier foil (Grainger 4UGU3, $76.2 \mu\text{m}$ thick) for R2R dry transfer experiments. Double-sided pressure-sensitive adhesive tape (Scotch Tape 6137H) was used for the bonding. Experiments were conducted to understand the effects of peeling speed and tension, and to identify the optimal peeling condition for the dry transfer process. The web speed was changed from 0.5 to 3 m min^{-1} with 0.5 m min^{-1} increments, and the peeling tension was varied among 5, 10, and 15 N. All resistance measurements in the study were performed with a nanovolt meter (Agilent 34420A). Scanning electron microscopy (FEI Quanta 650 ESEM) under the low vacuum mode and Raman spectroscopy with the 488 nm wavelength were used to confirm the presence of monolayer graphene after the R2R dry transfer. In the mobility and uniformity study, hydrogel (Red Dot,

BND-3M Medical Products 7 779 374 PT# 2360) with Ag/AgCl was used as the gate material. The measurement of the GFTEs was performed with Keysight B2902A.

Supporting Information

Supporting Information is available from the Wiley Online Library or from the author.

Acknowledgements

This material was based upon work supported by the National Science Foundation under Grant Nos. EEC-1160494 and CMMI-2041470. Any opinions, findings and conclusions or recommendations expressed in this material are those of the author(s) and do not necessarily reflect the views of the National Science Foundation. D.A. acknowledges the support of the Office of Naval Research Grant No. N00014-18-1-2706, and the Temple Foundation Endowed Professorship. W.L. also acknowledges the support of the Bob R. Dorsey Endowed Professorship.

Conflict of Interest

The authors declare no conflict of interest.

Author Contributions

N.H. and W.L. conceived the idea and designed the experiments. Q.Z., N.H., D.C., and W.L. designed and built the R2R transfer machine and implemented the tension and speed control. N.H., Q.Z., and D.K. performed the experiments. N.H. performed the simulation study. N.H., D.K., and W. L. analyzed the data. N.H., D.K., and W.L. wrote the manuscript. All authors discussed the results and provided comments for the manuscript.

Data Availability Statement

The data that support the findings of this study are available from the corresponding author upon reasonable request.

Keywords

flexible electronics, graphene-based field-effect transistor, large-scale CVD graphene, mechanical peeling, roll-to-roll dry transfer

Received: August 22, 2021

Revised: November 5, 2021

Published online:

[1] A. K. Geim, K. S. Novoselov, *Nat. Mater.* **2007**, *6*, 183.

[2] A. K. Geim, P. Kim, *Sci. Am.* **2008**, *298*, 90.

[3] D. R. Cooper, B. D'Anjou, N. Ghattamaneni, B. Harack, M. Hilke, A. Horth, N. Majlis, M. Massicotte, L. Vandsburger, E. Whiteway, V. Yu, *ISRN Condens. Matter Phys.* **2012**, *2012*, 1.

[4] S. Stankovich, D. A. Dikin, G. H. B. Dommett, K. M. Kohlhaas, E. J. Zimney, E. A. Stach, R. D. Piner, S. B. T. Nguyen, R. S. Ruoff, *Nature* **2006**, *442*, 282.

[5] R. R. Nair, P. Blake, A. N. Grigorenko, K. S. Novoselov, T. J. Booth, T. Stauber, N. M. R. Peres, A. K. Geim, *Science* **2008**, *320*, 1308.

[6] K. S. Kim, Y. Zhao, H. Jang, S. Y. Lee, J. M. Kim, K. S. Kim, J. H. Ahn, P. Kim, J. Y. Choi, B. H. Hong, *Nature* **2009**, *457*, 706.

[7] E. H. Hwang, S. D. Sarma, *Phys. Rev. B: Condens. Matter Mater. Phys.* **2008**, *77*, 115449-1.

[8] A. A. Balandin, S. Ghosh, W. Bao, I. Calizo, D. Teweldebrhan, F. Miao, C. N. Lau, *Nano Lett.* **2008**, *8*, 902.

[9] H. Chen, M. B. Müller, K. J. Gilmore, G. G. Wallace, D. Li, *Adv. Mater.* **2008**, *20*, 3557.

[10] Y. M. Lin, K. A. Jenkins, V. G. Alberto, J. P. Small, D. B. Farmer, P. Avouris, *Nano Lett.* **2009**, *9*, 422.

[11] X. Wang, L. Zhi, K. Müllen, *Nano Lett.* **2008**, *8*, 323.

[12] Y. Han, Z. Xu, C. Gao, *Adv. Funct. Mater.* **2013**, *23*, 3693.

[13] D. Akinwande, L. Tao, Q. Yu, X. Lou, P. Peng, D. Kuzum, *IEEE Nanotechnol. Mag.* **2015**, *9*, 6.

[14] T. Hesjedal, *Appl. Phys. Lett.* **2011**, *98*, 133106.

[15] I. Vlasiouk, P. Fulvio, H. Meyer, N. Lavrik, S. Dai, P. Datskos, S. Smirnov, *Carbon* **2013**, *54*, 58.

[16] G. Deokar, J. Avila, I. Rizado-Colambo, J. L. Codron, C. Boyaval, E. Galopin, M. C. Asensio, D. Vignaud, *Carbon* **2015**, *89*, 82.

[17] B. Lee, W. Chu, W. Li, *J. Micro Nano-Manuf.* **2020**, *8*, 031005-1.

[18] C. H. Lee, D. R. Kim, I. S. Cho, N. William, Q. Wang, X. Zheng, *Sci. Rep.* **2012**, *2*, 2.

[19] E. Suhir, *J. Appl. Mech. Trans. ASME* **2012**, *79*, 011010-1.

[20] Y. Zhang, Q. Liu, B. Xu, *Extrem. Mech. Lett.* **2017**, *16*, 33.

[21] Y. S. Chaug, J. E. Haubrich, M. Sereda, R. C. Liang, *Mater. Res. Soc. Symp. Proc.* **2004**, *814*, 213.

[22] S. Bae, H. Kim, Y. Lee, X. Xu, J. S. Park, Y. Zheng, J. Balakrishnan, T. Lei, H. Ri Kim, Y. Il Song, Y. J. Kim, K. S. Kim, B. Özyilmaz, J. H. Ahn, B. H. Hong, S. Iijima, *Nat. Nanotechnol.* **2010**, *5*, 574.

[23] T. Kobayashi, M. Bando, N. Kimura, K. Shimizu, K. Kadono, N. Umezu, K. Miyahara, S. Hayazaki, S. Nagai, Y. Mizuguchi, Y. Murakami, D. Hobar, *Appl. Phys. Lett.* **2013**, *102*, 023112-1.

[24] B. Jang, C. H. Kim, S. T. Choi, K. S. Kim, K. S. Kim, H. J. Lee, S. Cho, J. H. Ahn, J. H. Kim, *2D Mater.* **2017**, *4*, 024002.

[25] B. N. Chandrashekar, B. Deng, A. S. Smitha, Y. Chen, C. Tan, H. Zhang, H. Peng, Z. Liu, *Adv. Mater.* **2015**, *27*, 5210.

[26] Z. Y. Juang, C. Y. Wu, A. Y. Lu, C. Y. Su, K. C. Leou, F. R. Chen, C. H. Tsai, *Carbon* **2010**, *48*, 3169.

[27] H. Xin, Q. Zhao, D. Chen, W. Li, *J. Micro Nano-Manuf.* **2018**, *6*, 031004.

[28] A. Shivayogimath, P. R. Whelan, D. M. A. MacKenzie, B. Luo, D. Huang, D. Luo, M. Wang, L. Gammelgaard, H. Shi, R. S. Ruoff, P. Bøggild, T. J. Booth, *Chem. Mater.* **2019**, *31*, 2328.

[29] E. H. Lock, M. Baraket, M. Laskoski, S. P. Mulvaney, W. K. Lee, P. E. Sheehan, D. R. Hines, J. T. Robinson, J. Tosado, M. S. Fuhrer, S. C. Herna, S. G. Walton, *Nano Lett.* **2012**, *12*, 102.

[30] C. Xu, T. Yang, Y. Kang, Q. Li, T. Xue, K. M. Liechti, R. Huang, W. Qiu, *Adv. Mater. Interfaces* **2019**, *6*, 1901217.

[31] S. R. Na, S. Rahimi, L. Tao, H. Chou, S. K. Ameri, D. Akinwande, K. M. Liechti, *Nanoscale* **2016**, *8*, 7523.

[32] H. Xin, W. Li, *Appl. Phys. Rev.* **2018**, *5*, 031105.

[33] H. Xin, R. Borduin, W. Jiang, K. M. Liechti, W. Li, *Carbon* **2017**, *123*, 243.

[34] Q. Zhao, N. Hong, D. Chen, W. Li, in *Proc. ASME 2020 15th Int. Manuf. Sci. Eng. Conf.*, **2020**, 84256, MSEC2020-8507.

[35] H. Xin, *Design and Analysis for Roll-to-Roll Graphene Transfer*, Ph.D. dissertation, The University of Texas at Austin, Austin, Texas, USA **2017**.

[36] S. R. Na, X. Wang, R. D. Piner, R. Huang, C. G. Willson, K. M. Liechti, *ACS Nano* **2016**, *10*, 9616.

[37] Y. Wei, *J. Mech. Phys. Solids* **2014**, *70*, 227.

[38] D. Kireev, M. Brambach, S. Seyock, V. Maybeck, W. Fu, B. Wolfrum, A. Offenhäuser, *Sci. Rep.* **2017**, *7*, 6658.

- [39] X. Zhang, Q. Jing, S. Ao, G. F. Schneider, D. Kireev, Z. Zhang, W. Fu, *Small* **2020**, *16*, 1902820.
- [40] M. H. Alam, Z. Xu, S. Chowdhury, Z. Jiang, D. Taneja, S. K. Banerjee, K. Lai, M. H. Braga, D. Akinwande, *Nat. Commun.* **2020**, *11*, 3203.
- [41] L. H. Hess, M. Seifert, J. A. Garrido, *Proc. IEEE* **2013**, *101*, 1780.
- [42] J. D. Caldwell, T. J. Anderson, J. C. Culbertson, G. G. Jernigan, K. D. Hobart, F. J. Kub, M. J. Tadjer, J. L. Tedesco, J. K. Hite, M. A. Mastro, R. L. Myers-Ward, C. R. Eddy, P. M. Campbell, D. K. Gaskill, *ACS Nano* **2010**, *4*, 1108.